Chemistry–A European Journal
Research Article
doi.org/10.1002/chem.202104301
Chemistry Europe
European Chemical Societies Publishing
www.chemeurj.org

# Tetra-Substituted *p-Tert*-Butylcalix[4]Arene with Phosphoryl and Salicylamide Functional Groups: Synthesis, Complexation and Selective Extraction of f-Element Cations

Florian Glasneck,[a] Quirina I. Roode-Gutzmer,[b] Thorsten Stumpf,[b] and Berthold Kersting*[a]

**Abstract:** A new series of lanthanide (**1**–**5**) and uranyl (**6**) complexes with a tetra-substituted bifunctional calixarene ligand $\mathbf{H_2L}$ is described. The coordination environment for the $Ln^{3+}$ and $UO_2^{2+}$ ions is provided by phosphoryl and salicylamide functional groups appended to the lower rim of the *p-tert*-butylcalix[4]arene scaffold. Ligand interactions with lanthanide cations (light: $La^{3+}$, $Pr^{3+}$; intermediate: $Eu^{3+}$ and $Gd^{3+}$; and heavy: $Yb^{3+}$), as well as the uranyl cation ($UO_2^{2+}$) is examined in the solution and solid state, respectively with spectrophotometric titration and single crystal X-ray diffractometry. The ligand is fully deprotonated in the complexation of trivalent lanthanide ions forming di-cationic complexes 2:2 M:**L**, $[Ln_2(\mathbf{L})_2(H_2O)]^{2+}$ (**1**–**5**), in solution, whereas uranyl formed a 1:1 M:**L** complex $[UO_2(\mathbf{L})(MeOH)]_\infty$ (**6**) that demonstrated very limited solubility in 12 organic solvents. Solvent extraction behaviour is examined for cation selectivity and extraction efficiency. $\mathbf{H_2L}$ was found to be an effective extracting agent for $UO_2^{2+}$ over $La^{3+}$ and $Yb^{3+}$ cations. The separation factors at pH 6.0 are: $\beta_{UO_2^{2+}/La^{3+}} = 121.0$ and $\beta_{UO_2^{2+}/Yb^{3+}} = 70.0$.

## Introduction

Rare-earth elements (REE), which include all the lanthanides, yttrium and scandium, are important metals used in the production of permanent magnets, luminescent materials, ceramic supports for exhaust emission catalysts, catalysts for petroleum cracking, de-oxygenation of steel, and many other areas. To manage the turnaround in the energy policy, the demand for permanent magnets for wind turbines and electric vehicle technology is expected to increase significantly. Circumventing possible supply bottlenecks of REEs necessitates the development of recycling technologies, for example, recent work by Lorenz et al. (2019).[1] Even though Australia now meets 10% of the international demand for REEs, until 2019 China produced 70–80% of the world's REEs from primary resources.[2] Producers of rare-earths are required to adhere to radiation protection measures. It is therefore essential to ensure radioactive decontamination prior to recovering the REEs,[3] which is always associated with radioactive uranium and thorium. It is therefore essential to ensure radioactive decontamination prior to recovering the REEs. Due to similar chemical behaviour and ionic radii of adjacent lanthanide ions, their separation and purification is complex, laborious, and cost-intensive. Furthermore, lanthanides for magnetic and luminescent material applications are required to be of high purity. Current commercial extractants include organophosphorus acids, such as di-(2-ethylhexyl)-phosphoric acid (D2EHPA), which require saponification with ammonia to improve separation selectivity and extraction efficiency. To reduce the pollution that is associated with the rare-earth hydrometallurgical industry,[4] more selective extractants, such as calixarenes and other polydentate chelate ligands,[5–7] are sought after. Not only is it important to remove radiotoxic actinides from rare-earth extraction streams, but removing lanthanides from long-lived actinides in high level nuclear waste streams is becoming more relevant in nuclear waste disposal processes. By virtue of some lanthanides possessing considerably high thermal neutron-capture cross-sections ($^{157}$Gd, abundance 15.7%, $254 \cdot 10^3$ barns, $^{151}$Eu, abundance 47.8%, $9.23 \cdot 10^3$ barns),[8] it is necessary to remove these lanthanides from plutonium-containing spent nuclear fuel prior to transmutation in fast reactors to produce shorter-lived radionuclides. Current extraction technology for the separation of actinides from nuclear waste does not possess sufficient selectivity nor extraction yields.[9–11]

The potential for calixarenes to be employed as an extracting agent for the separation and purification of lanthanides was first demonstrated in 1987.[12] Since then the literature abounds with investigations into designing calixarenes for the selective extraction and separation of actinides and lanthanides.[13] Similar to the industrially applied organophosphorus compounds to extract lanthanides, calixarenes have been functionalized with phosphonic acid and phosphine oxide

[a] Dr. F. Glasneck, Prof. Dr. B. Kersting
Institute of Inorganic Chemistry
Leipzig University
Johannisallee 29, 04103 Leipzig (Germany)
E-mail: b.kersting@uni-leipzig.de
[b] Q. I. Roode-Gutzmer, Prof. Dr. T. Stumpf
Institute of Resource Ecology
Helmholtz-Zentrum Dresden-Rossendorf
Bautzner Landstrasse 400, 01328 Dresden (Germany)
E-mail: t.stumpf@hzdr.de

Supporting information for this article is available on the WWW under https://doi.org/10.1002/chem.202104301

© 2021 The Authors. Chemistry - A European Journal published by Wiley-VCH GmbH. This is an open access article under the terms of the Creative Commons Attribution Non-Commercial NoDerivs License, which permits use and distribution in any medium, provided the original work is properly cited, the use is non-commercial and no modifications or adaptations are made.


© 2021 The Authors. Chemistry - A European Journal published by Wiley-VCH GmbH

groups.[14,15] Analogous examples with carboxylic acid derivatives as extracting agents for lanthanides are also known.[16] The extraction performance and selectivity, however, were in the best cases comparable with D2EHPA. Calixarenes furnished with additional functional groups have been developed for liquid-liquid/solvent extraction. Improved selectivity for trivalent actinides over lanthanides could be achieved with picolinamide-functionalized calix[*n*]arenes ($n=4$, 6, 8), which was explained by the strong interaction of the nitrogen donor group and soft actinides.[17] Calixarenes functionalized with phosphoryl and/or amide groups have demonstrated significant selectivity and appreciable extraction capacity.[18] Trivalent f-element ions can be efficiently extracted with bidentate ligands with hard O-donors.[7] When such ligands are additionally furnished with soft N-donors, selectivity for actinides over lanthanides is achieved due to differences in coordination behaviour of 4f- and 5f-cations.[6,7,14] In previous work we were able to append N- and O-donors on a calixarene scaffold[19] in such a way as to achieve a very high selectivity for adjacent lanthanides with separation factors of $ß_{Er/Dy}=4.4$ and $ß_{Dy/Tb}=2.5$ (Schreiter et al.[20,21]). Furthermore, we achieved excellent separation between uranyl and trivalent lanthanide cations in liquid-liquid extraction experiments.[22] It could also be demonstrated that the synthesis of such calixarenes can be up-scaled to pilot-plant scale.[21] In this paper we describe the synthesis, spectroscopic properties and solid state structures of a series of new lanthanide and uranyl complexes (**1**–**6**) derived from the tetrapodal ligand system **$H_2$L** bearing two phosphoryl groups and two salicylamide groups on the lower rim. The effects of the ligand modification on the extraction properties are discussed and compared with those of the previously reported neutral ligand **L′** (Scheme 1).[23]

## Results and Discussion

Appending different substituents on the lower rim of the ligand precursor *p-tert*-butylcalix[4]arene requires several synthetic steps. The precursor calix[4]arene compounds, as well as the required substituent educts were intentionally synthesized in-house so as to enable an up-scaled synthesis with the objective of possible technology transfer. Furthermore, phosphoryl compounds with suitable leaving groups are in most cases not commercially available. In preliminary investigations it became quickly apparent that the order in which the substitution takes place to achieve a tetra-substituted calix[4]arene with two different functional groups, is very decisive in achieving the desired product. We developed a synthetic procedure in which the phosphoryl groups were appended first in the 1,3-position, followed by the second reaction step, in which the nitrogen-containing carboxylic acid ester groups were added in the 2,4-position.[23] The synthesis of the substituent educts and precursor calix[4]arenes are described by Glasneck et al.[23] and with additional synthesis and analytical details in the Supporting Information in this paper.

The synthesis of **$H_2$L** follows by converting the phosphoryl and amine derivative **1′** with salicylic acid pentafluorophenyl ester in chloroform (Scheme 2). After purifying in a chromatography column, the pure product was obtained with a yield of 56 %.

The $^1$H NMR of **$H_2$L** in $CD_2Cl_2$ (Figures S1 and S2, Supporting Information) reveals two characteristic AB systems for the Ar–$CH_2$–Ar groups, which is indicative of a $C_2$-symmetric *cone* conformation. One $^{31}$P NMR signal at 32.4 ppm (Figures S1 and S4, Supporting Information) is also in agreement with $C_2$ symmetry. The ESI (+) mass spectrum of **$H_2$L** (Figure S5, Supporting Information) shows a dominant signal at $m/z=$ 1353.7 for the $Na^+$ adduct. Absorption bands at 203 nm and 303 nm with a shoulder at 287 nm are observed in the UV-vis spectrum of **$H_2$L** (Figure S6, Supporting Information) in acetonitrile. These bands are indicative of $\pi$–$\pi^*$ and $n$–$\pi^*$ transitions within the aromatic rings of the calixarene scaffold (287 nm) and the conjugated amide group (303 nm), respectively.[24]

Crystals of **$H_2$L**·3MeCN suitable for X-ray crystallographic analysis were obtained by slow evaporation from a solution containing a solvent mixture of dichloromethane and acetonitrile. In the solid state the calix[4]arene adopts a *flattened cone* conformation similar to that seen for the dinitrile derivative **c** ("dinitrile derivative" may alternatively be referred to as precursor to **1′**)(Figure S7),[23] with the phosphoryl-substituted aromatic rings (A,B) being nearly parallel to each other. The deviation from the ideal *cone* conformation can be ascribed to a network of intra- and intermolecular hydrogen bonds between substituents. The pendant salicylamide units are almost perfectly planar due to intramolecular OH···O=C

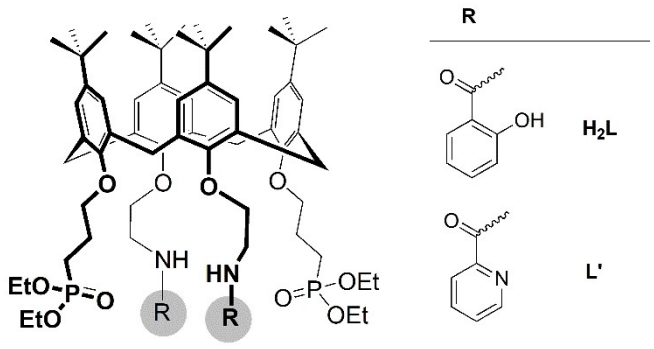


**Scheme 1.** Neutral ligand, **L′**,[23] and ligand system **$H_2$L** (this work).

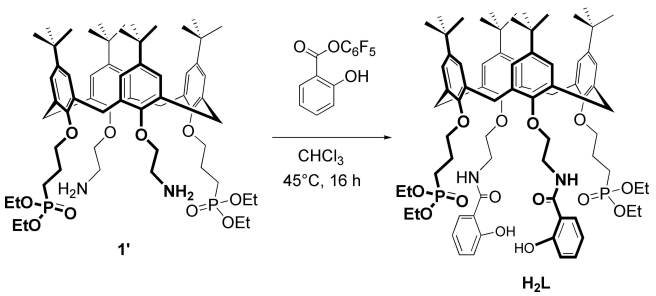


**Scheme 2.** Synthesis of **$H_2$L**.


© 2021 The Authors. Chemistry - A European Journal published by Wiley-VCH GmbH

hydrogen bonds (O12···O11, O14···O13), typical for o-hydroxyaryl amides.[25,26] The structure is further stabilized by intramolecular (N1···O5) and intermolecular N2···O8′ hydrogen bonding interactions involving the amide NH hydrogen and phosphoryl P=O oxygen atoms to generate dimeric units as illustrated in Figure 1. Based on the observed bonding lengths and angles, the hydrogen bonds and electrostatic interactions within the molecule is anywhere between moderate and considerable according to the classification of Jeffrey and Saenger.[27] The packing coefficient of the acetonitrile solvent as guest molecule in the cavities of this structure is calculated using VEGA ZZ[28] to amount to 0.53, which lies in the range $0.55 \pm 0.09$ postulated by Mecozzi and Rebek,[29] for optimal binding of guest molecules by self-assembled or covalently linked capsules. In other words, the three MeCN molecules perfectly fit the voids produced by the packing of the calixarene ligands.

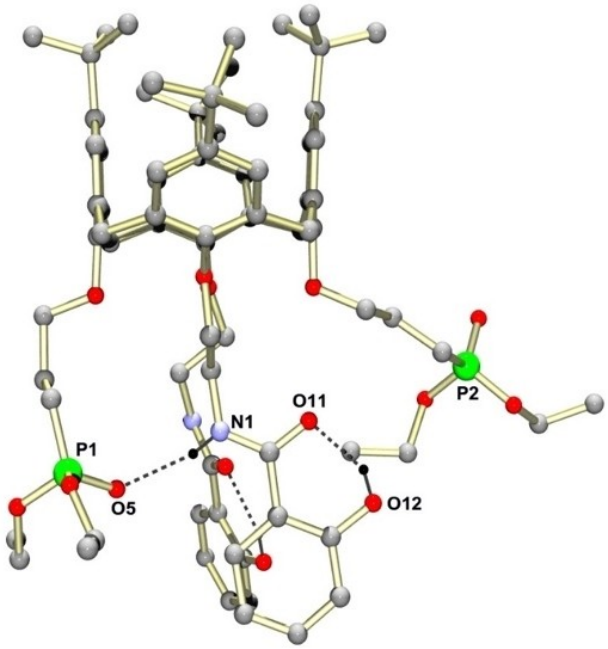


**Figure 1.** Solid-state structure of compound $\mathbf{H_2L}$ as determined by single-crystal X-ray diffraction, showing one of the two crystallographically independent but chemically identical molecules of $\mathbf{H_2L}$. Selected distances [Å]: O11···O12 2.496, O5···N1 2.994.

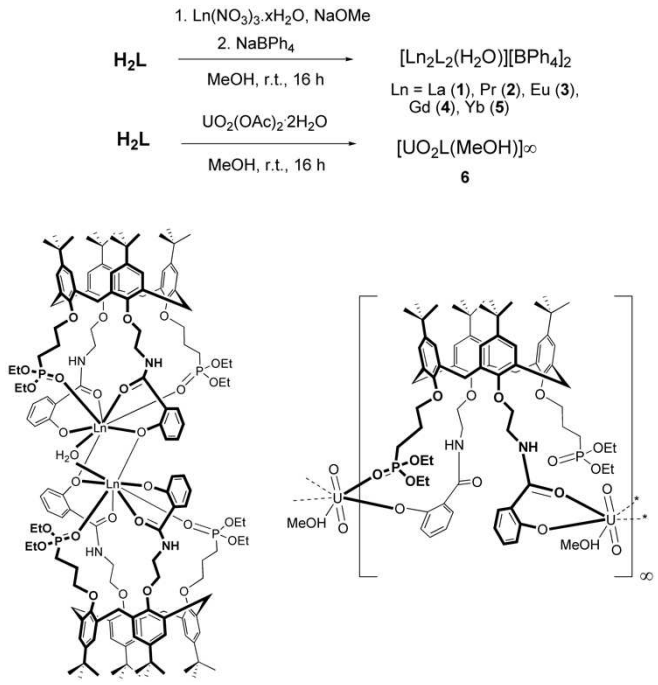


**Scheme 3.** Synthesis of metal ligand complexes **1**–**6.**

## Synthesis and characterization of complexes

Complexation studies of $\mathbf{H_2L}$ were conducted with selected rare earth elements ($La^{3+}$, $Pr^{3+}$, $Eu^{3+}$, $Gd^{3+}$ and $Yb^{3+}$) as well as the uranyl cation, $UO_2^{2+}$, in order to investigate the coordination properties of the ligand. Treatment of $\mathbf{H_2L}$ with $Ln(NO_3)_3 \cdot nH_2O$ and sodium methoxide as a base in MeOH (Scheme 3) invariably provides di-cationic $[Ln_2(\mathbf{L})_2(H_2O)]^{2+}$ complexes (**1**–**5**). Salt metathesis with $NaBPh_4$ provides the corresponding $BPh_4^-$ salts. The yields range from 49 to 91%. The presence of a 2:2 M:**L** stoichiometry is indicated by ESI-MS spectra, which show a single signal for the $[Ln_2\mathbf{L}_2]^{2+}$ species, except for the $Yb^{III}$ complex (**5**), which also reveals a signal for a mono-cation $[Yb\mathbf{L}]^+$ (Figures S8–S17, Supporting Information). It is assumed that this species is a dissociation product of the dimer, formed during the ionization process in the mass spectrometer. $\mathbf{H_2L}$ was also allowed to react with uranyl (VI) acetate dihydrate in methanol. No extra base was added. A yellow solid, analysed as $[UO_2(\mathbf{L})(MeOH)]_\infty$ (**6**) was isolated in 68% yield. The ESI (+) mass spectrum of **6** in methanol shows a signal for the sodium adduct $[(UO_2)\mathbf{L} + Na^+]$ at $m/z = 1621.7$ with the correct isotopic ratio (Figures S18 and S19, Supporting Information).

All complexes are hygroscopic, taking up varying amounts of $H_2O$ upon standing in air. $H_2O$ is included in the initially isolated products. Upon crystallization from $MeOH/CH_2Cl_2$, the $H_2O$ molecules are replaced by MeOH molecules. All new complexes gave satisfactory elemental analysis and were further characterized by ATR-IR spectroscopy (Figures S20-S25, Supporting Information), UV-vis spectrophotometry (Figures S26-S31, Supporting Information), and in the case of **1**, **3**, **4**, and **6** also by X-ray crystallography. The ATR-IR spectra of the $Ln^{3+}$ complexes **1**–**5** are almost identical. The most prominent features are the N–H stretching vibrations of the amide groups which are detected in the range between 3350 $cm^{-1}$ and 3450 $cm^{-1}$. The ν(CO) band for the amide groups appears at a lower frequency in comparison to the free ligand (1608 $cm^{-1}$), which is indicative of coordination to $Ln^{3+}$. P=O stretches could not be located unambiguously due to their low intensity and overlapping resonances from other groups. The coordination of the salicylamide unit is also reflected in the UV-vis spectra. The intra-ligand absorption bands are shifted bathochromically upon $Ln^{3+}$ ion binding from 303 nm to 323 nm. The IR spectrum of **6** reveals two signals for the C=O stretching vibrations, 1645 $cm^{-1}$ and 1610 $cm^{-1}$. The former is only slightly


© 2021 The Authors. Chemistry - A European Journal published by Wiley-VCH GmbH

shifted compared to **$H_2$L** and is assigned to the non-coordinating carbonyl group, while the latter is assigned to the amide (CO) group bound to the $UO_2^{2+}$ di-cation. An absorption band at 1540 $cm^{-1}$ corresponds to the C–N-H deformation vibration of the amide group. The band at 914 $cm^{-1}$ is attributed to the asymmetric stretching vibration of the $[O{=}U{=}O]^{2+}$ di-cation. As for **1**–**5**, the ν(PO) band could not be assigned unequivocally. The coordination polymer **6** exhibits extremely low solubility in all common solvents ($CH_2Cl_2$, $CHCl_3$, MeOH, EtOH, i-PrOH, THF, MeCN, DMSO, DMF, $Et_2O$, *n*-hexane, acetone) such that no solution UV-vis spectra could be recorded. The diffuse reflectance spectrum of solid complex **6** dispersed in $BaSO_4$ matrix reveals an absorption maximum at 314 nm. This absorbtion maximum has a tail that extends into the visible (~500 nm) with no clear maximum (Figure S32). The diffuse reflectance spectrum of the free ligand has no absorptions in the visible.

### Molecular structures of metal ligand complexes

Single-crystals of $[Ln_2L_2(\mu\text{-}H_2O)](BPh_4)_2 \cdot x$MeOH (Ln=La (**1**) (x~14), Eu (**3**) (x~12), and Gd (**4**) (x~13)) suitable for X-ray crystallographic analysis were obtained by slow evaporation from a mixed $CH_2Cl_2$/MeOH solvent system. The lanthanide compounds are isostructural, crystallizing in the triclinic space group *P-1* with two formula units per unit cell (Table S1, Supporting Information). Figure 2 illustrates the structure of the di-cationic $Eu^{3+}$-complex **3**, which is representative for all the lanthanides. The Eu ions are eightfold coordinated, being surrounded by two phosphoryl O, two carbonyl O, two bridging and one terminal phenolate O atom of the deprotonated supporting ligand. A bridging $H_2O$ ligand completes the coordination geometry, which is best described as distorted bi-augmented trigonal prismatic according to the SHAPE[30] symmetry factors (Table S2, Supporting Information). The two coordination polyhedra are joined via one trigonal face. The Ln···Ln distances are 3.979(1) Å (**1**), 3.831(1) Å (**3**), and 3.842(1) Å (**4**), a typical distance for triply bridged Ln structures.[31,32] Selected metal ligand bond lengths are listed in Table S3 (Supporting Information). The Ln–O bonds in **1** are significantly longer than those in **3** and **4**, consistent with the larger ionic radius of the $La^{3+}$ ion.[33] The aqua ligand forms the longest Ln–O bonds ranging from 2.772(7) Å in **1** to 2.656(3) Å in **4**. The Ln–O bonds involving the monodentate phenolate groups exhibit average bond lengths of 2.418 Å (**1**), 2.308 Å (**3**), and 2.283 Å (**4**), while the bridging phenolate groups form longer Ln–O bonds at 2.524 Å (**1**), 2.418 Å (**3**), and 2.419 Å (**4**). Throughout the series, the Ln–phosphoryl–O bonds are significantly shorter than the Ln–carbonyl-O distances, in agreement with the strong affinity of P=O-donor groups to the rare earth elements.[34] The mean difference of the Ln–OP versus the Ln–OC bonds amounts to 0.059 Å for **1**, 0.037 Å for **3**, and 0.067 Å for **4**. The deprotonated salicylamide groups form six-membered chelate rings with the $Ln^{3+}$ ions. The corresponding O–Ln–O angles increase across the series (mean values: 69.4° (**1**), 72.2° (**3**), 74.1° (**4**)), which is consistent with a decreasing ionic radius (Table S4, Supporting Information). The amide group is not coplanar with the phenolate group as is the case with **$H_2$L**. The average Ln–O–Ln bond angles for the phenolate groups are: 104.1° (**1**), 104.8° (**3**), and 105.1° (**4**). The Ln–μ($OH_2$)–Ln angles are ca. 10° smaller.

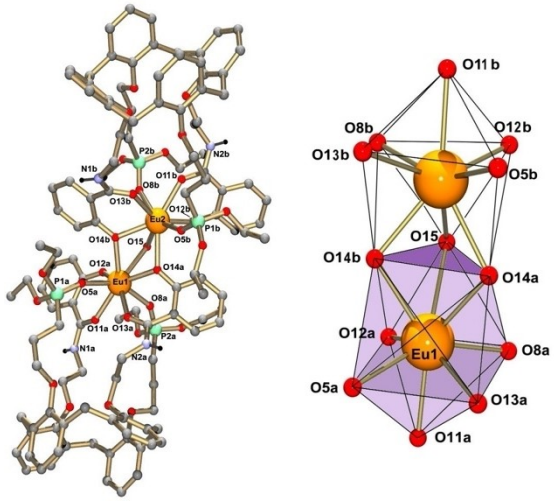


**Figure 2.** Left: Single-crystal X-ray diffraction structure of the $[Eu_2(\mathbf{L})_2(\mu\text{-}H_2O)]^{2+}$ dication in crystals of **3**·14MeOH (ball-and-stick model). *Tert*-butyl groups and hydrogen atoms (except for NH) are omitted for clarity. Right: Coordination environments of the Eu ions in the $[Eu_2(\mathbf{L})_2(\mu\text{-}H_2O)]^{2+}$ di-cations.

A comparison of the complexation behaviour of the ligands **L′** and **$H_2$L** is appropriate at this stage. Previously, we have described the synthesis and structures of several $Ln^{3+}$ complexes supported by the neutral ligand **L′**.[23] This ligand was found to form exclusively 1:1 complexes of the type $[Ln(\mathbf{L}')(NO_3)_2]^+$. As in the case of the present complexes, the $Ln^{3+}$ cations are invariably coordinated in a tetrapodal fashion by phosphoryl O, amide O, and picolinamide N atoms from **L′**. In contrast to the phenolate group in the complexes of **$H_2$L**, the pyridyl nitrogen in **L′** has only one lone pair of electrons available for coordination. Therefore, **L′** cannot act as bridging ligand, such that only monomeric complexes from. The finding that the salicylamide O atoms can act as bridging ligands suggests that these complexes may also be interesting to investigate as precursor for the synthesis of polynuclear complexes or for supramolecular architectures.

Yellow prisms of $[UO_2(MeOH)(\mathbf{L})]_n \cdot 5n$MeOH (**6**·5MeOH) were obtained by slow evaporation from methanol. This complex crystallizes in the orthorhombic space group *Pbca* with 8 formula units per unit cell (Table S1, Supporting Information). The crystal structure determination revealed the presence of a one-dimensional coordination polymer, with each $UO_2^{2+}$ di-cation linking two doubly-deprotonated calix[4]arene ligands. Figure 3 displays a section of the polymeric structure. Each uranyl ion is bonded to one phosphoryl-O and one salicylamide-O atom of one calix[4]arene ligand and to two O atoms of a chelating salicylamide residue of another calix[4]arene ligand. A MeOH molecule completes the compressed pentagonal bipyramidal coordination geometry of the U atom (with O15 and O16 in axial positions). Thus, one phosphoryl unit per


© 2021 The Authors. Chemistry - A European Journal published by Wiley-VCH GmbH

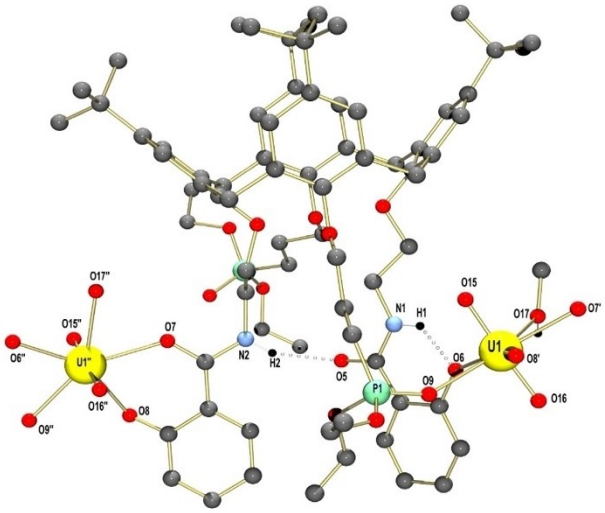


**Figure 3.** Molecular structure of the [$UO_2$(MeOH)(**L**)] complex in crystals of **6**·5MeOH (ball-and-stick model). *Tert*-butyl groups and hydrogen atoms (except for NH) are omitted for clarity.

calix[4]arene remains uncoordinated in this case. The immediate coordination environment of the $UO_2^{2+}$ cation is displayed in Figure 4 along with selected bond lengths and angles. The uranyl cation is approximately linear with an O–U–O angle of 177.5(2)°. The average U=O bond length of 1.769 Å is normal.[35]

The sum of the O–U–O bond angles for the five equatorial ligands amounts to 360.1°, which reveals an approximately perfect planarity of the base area of the bipyramid. The SHAPE symmetry factor amounts to 1.664 for the pentagonal bipyramidal geometry (Table S2, Supporting Information). The chelating salicylamide group forms a six-membered ring with the $U^{6+}$ centre, in which the O–U–O angle is 69.6(2)°, quite similar to the corresponding O–Ln–O angles in **1**, **3**, and **4** (Table S3, Supporting Information). The complexation of the cations leads to a tilting of the amide group with respect to the

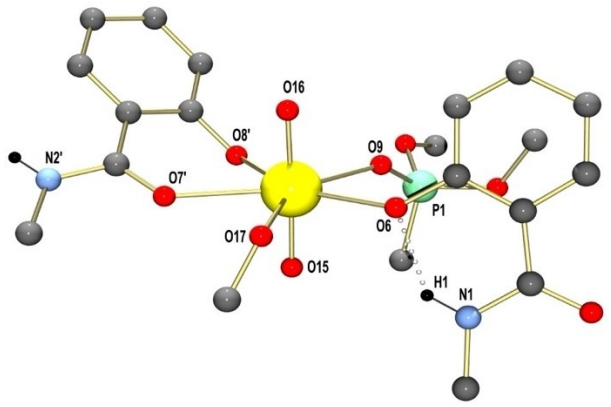


**Figure 4.** Coordination environments of the $UO_2^{2+}$ ions in **6**. Selected bond lengths /Å and angles /°: U1–O6 2.292(4), U1–O7′ 2.431(4), U1–O8′ 2.279(5), U1–O9 2.417(4), U1–O15 1.775(4), O16–U1 1.763(4), U1–O17 2.448(6), O15–U1–O16 177.4(2), O8′–U1–O7′ 69.6(2). Symmetry codes used to generate equivalent atoms: 0.5−*x*, 0.5+*y*, *z* (′), 0.5−x, −0.5+y, z (″).

phenolate ring and a deviation from the planarity of the conjugated π system. The bond lengths of the equatorial ligands are significantly longer than those of the oxo ligands. The deprotonated phenolic hydroxyl groups have shorter bond lengths (mean value 2.287 Å) than those of the uncharged phosphoryl, carbonyl and methanol groups, which each have a distance larger than 2.4 Å to the metal centre. All observed bond lengths are in accordance with those described in the literature.[36]

The complexation of the uranyl cation requires less donor atoms than those supplied by **$H_2$L**. Thus in contrast to $Ln^{3+}$ cations, some potential binding sites of the ligand do not participate in the complexation and there is no formation of isolated, mononuclear complex molecules. The non-coordinating carbonyl oxygen atom O11 forms an intramolecular hydrogen bond with the amide group CON(2)H. Compared to the molecular structure of the free ligand **$H_2$L**, a rotation of the C–C bond between the carbonyl carbon atom and the aromatic phenol ring takes place to accommodate this hydrogen bonding interaction. Another hydrogen bond exists between the hydrogen atom at N1 and the phenolate oxygen atom O12 of the monodentate salicylamide group.

## Spectrophotometric titration studies

UV-vis spectrophotometric batch titrations were carried out in order to study the complexation reactions of **$H_2$L** with $La^{3+}$, $Pr^{3+}$, $Eu^{3+}$, $Gd^{3+}$, and $Yb^{3+}$ ions in the solution state. For comparison, a similar setup and similar experimental conditions as used previously for the titrations of the ligand **L′** (bearing picolinamide units, cf. Scheme 1) was selected herein too.[23] Thus, all batch experiments were carried out at constant ionic strength ($10^{-2}$ M $n$$Bu_4NPF_6$) and constant ligand concentrations ($2.5\cdot10^{-5}$ M) in pure acetonitrile. Although the conducting salt will not dissociate completely under these experimental conditions the large molar excess still assures a constant ionic strength during the titration studies.[37] Also, for the present ligand, the complexation studies were carried out in the presence of 5.0 equivalents of triethylamine in order to maintain a constant basic pH value. It is assumed that **$H_2$L** is present in its doubly deprotonated form (**$L^{2-}$**) under these conditions (p$K_a$(salicylamide) = 8.37).[38]

The titration of **$L^{2-}$** with $La(NO_3)_3\cdot6H_2O$ is shown in Figure 5 and is representative for titrations of all lanthanides examined (see Figure S32, Supporting Information, for the spectrophotometric titration of **$L^{2-}$** with $Yb^{3+}$ in solution). A solution of the free ligand exhibits an absorption band at 303 nm and a shoulder at ~270 nm. These two absorption bands are tentatively assigned to the π-π* transitions centred on the phenolate rings of the salicylamide units and the calix[4]arene moiety, respectively, since the free components exhibit characteristic π-π transitions at very similar wavelengths.[39] The addition of aliquots of $La(NO_3)_3$ (from 0.1 to 7.0 equiv.) leads to clear changes in the UV-vis ligand spectra. The band at 303 nm for **$L^{2-}$** vanishes with increasing $La^{3+}$ concentration, and a new band develops with a maximum at 326 nm. An isosbestic point


© 2021 The Authors. Chemistry - A European Journal published by Wiley-VCH GmbH

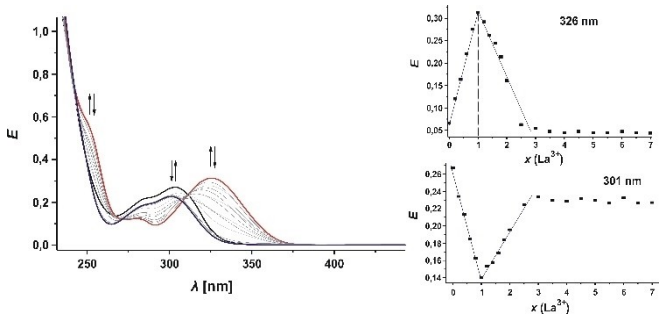


**Figure 5.** Left: Spectrophotometric titration of the calixarene ligand $\mathbf{L}^{2-}$ ($10^{-5}$ M) with varying amounts of $La(NO_3)_3 \cdot 6H_2O$ in $CH_3CN$ at constant ionic strength ($10^{-2}$ M $(^nBu)_4NPF_6$, $T = 298$ K) in the presence of $NEt_3$ ($10^{-4}$ M). The black curve refers to the free ligand. The red curve corresponds to a molar ratio of $La^{3+}/\mathbf{L}^{2-} = 1.0$, with the blue curve representing the final molar ratio of $La^{3+}/\mathbf{L}^{2-} = 7.0$. Right: Evolution of absorbance values at 326 and 301 nm as a function of the $[La^{3+}]/[\mathbf{L}^{2-}]$ molar ratio.

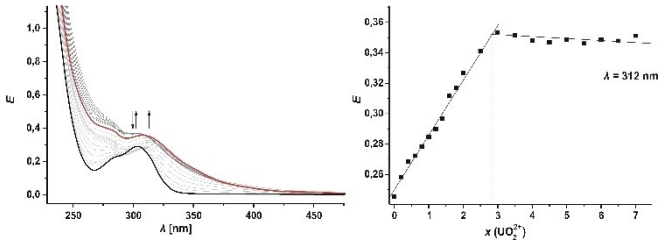


**Figure 6.** Left: Spectrophotometric titration of the calixarene ligand $\mathbf{H_2L}$ ($10^{-5}$ M) with varying amounts of $UO_2(NO_3)_2 \cdot 6H_2O$ in $CH_3CN$ at constant ionic strength ($10^{-2}$ M $^nBu_4NPF_6$, $T = 298$ K) in the presence of $NEt_3$ ($10^{-4}$ M). The black curve refers to the spectrum of the free ligand. The red curve corresponds to a molar ratio of $UO_2^{2+}/\mathbf{L}^{2-} = 1.0$. The blue curve corresponds to a final molar ratio of $UO_2^{2+}/\mathbf{L}^{2-} = 3.0$. Right: Evolution of absorbance values at $\lambda = 312$ nm versus the $[UO_2^{2+}]/[\mathbf{L}^{2-}]$ molar ratio.

at ~310 nm indicates the existence of a new species and suggests that the binding of $La^{3+}$ occurs at a single equilibrium.

To determine the stoichiometry of the resulting species the spectroscopic data were analysed in terms of the mole ratio method as described by Yoe and Harvey.[40] As can be seen from the absorbance plot *versus* molar ratio $[La^{3+}]/[\mathbf{L}^{2-}]$ at 326 nm in Figure 5, absorption increases steadily up to a molar ratio of about unity and then decreases again. This is indicative of the formation of a species with 1:1 stoichiometry. At a $[La^{3+}]/[\mathbf{L}^{2-}]$ ratio of unity the overall spectrum resembles that of the isolated $La^{3+}$ complex **1**. This suggests that this complex also exists in the solution state. With further addition of $La^{3+}$ ions, the intensity of the absorption band at 326 nm decreases again. This indicates the formation of a new species. From approx. 2.5 equiv. of added $La^{3+}$ salt no further changes in the spectra occur and the formation of the complex species seems to be completed. The final spectra are similar but not identical to that of the free ligand. We believe that the addition of further $La^{3+}$ ions leads to the formation of mixed-ligand complexes with $Ln/\mathbf{L}^{2-}$ ratios > 1, where phenolate O atoms of the salicylamide units are involved in a bridging coordination mode. IR spectroscopic and ESI mass spectrometric investigations of the solutions with high $M/\mathbf{L}^{2-}$ ratios > 1 did not lead to any results that could be evaluated. In the spectrophotometric titration of $\mathbf{H_2L}$ with the $Eu^{3+}$ solution, various parameters were varied in order to examine possible interactions that may differ. No change in the complexation behaviour could be observed by spectrophotometric titration.

The titration of $\mathbf{L}^{2-}$ with $UO_2(NO_3)_2 \cdot 6H_2O$ is shown in Figure 6. The addition of aliquots of $UO_2(NO_3)_2$ (from 0 to 3 equiv.) leads to clear changes in the UV-vis ligand spectra. The band at 303 nm for $\mathbf{L}^{2-}$ shifts bathochromically to 312 nm and also gains intensity with increasing $UO_2^{2+}$ concentration. The mole ratio method was applied in order to determine the stoichiometry of the resulting species. As can be seen from Figure 6, the plot of the absorbance value at 312 nm versus molar ratio $[UO_2^{2+}]/[\mathbf{H_2L}]$ increases steadily up to a molar ratio of about 3 and then remains constant. This molar ratio differs from that determined by X-ray crystallography for **6** and shows that the solution species has a different composition.

Little information is available on the stability constants of 1:1 lanthanide complexes involving tetrapodal calix[4]arenes with dangling phosphonate donor arms. The binding constants of $Ln^{3+}$-complexes with **L'** lie in the range log $K = 6$–$9$.[23] The stability constants of the 1:1 complexes presented herein are believed to lie in a similar range.

## Extraction

Given the different coordination behaviour of $\mathbf{H_2L}$ towards $Ln^{3+}$ and $UO_2^{2+}$ cations (and the technological importance of separation of radiotoxic 5f from rare-earth elements), it was of interest to examine the extraction properties of $\mathbf{H_2L}$ towards these cations. Figure 7 clearly illustrates the favourable extraction of the uranyl cation with $\mathbf{H_2L}$ over the trivalent lanthanide cations. While the extraction of $La^{3+}$ and $Yb^{3+}$ into the organic phase is only significant at pH > 5.5, there is a very sharp

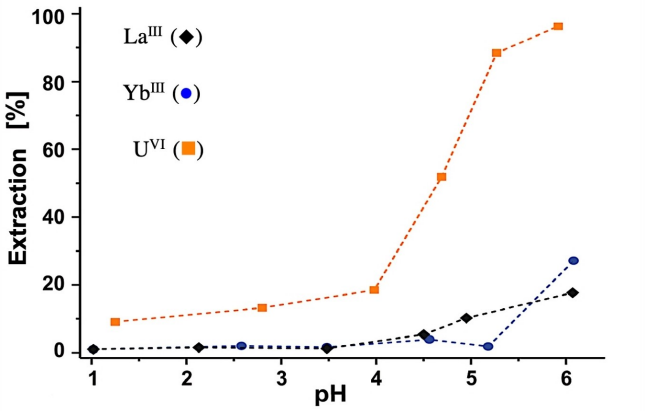


**Figure 7.** Extraction of single metal cations with $\mathbf{H_2L}$ as a function of pH at $T = 298$ K. Organic phase: $[\mathbf{H_2L}] = 10^{-2}$ mol/L in $CHCl_3$. Aqueous phase: $[La^{3+}]$, $[Yb^{3+}]$, $[UO_2^{2+}]$ each with a concentration of $10^{-4}$ mol/L buffered with $H_3BO_3/Na_2B_4O_7$ ($10^{-2}$ mol/L in $H_2O$). Extraction: 15 min. Equilibration: 30 min.


© 2021 The Authors. Chemistry - A European Journal published by Wiley-VCH GmbH

increase in the extraction of $UO_2^{2+}$ already occurring in the pH range of 4.0–5.0.

The separation factor $\beta_{A/B}$ for two different metals A and B at a given pH value is defined as

$$\beta_{A/B} = D_A/D_B.$$

Here, $D_A$ and $D_B$ are the distribution coefficients of the metals at a given pH after the extraction.[5] They are defined as the ratios of the total equilibrium concentrations of the metals in the organic and the aqueous phase, respectively:

$$D_A = [A]_{org}/[A]_{aq},\ D_B = [B]_{org}/[B]_{aq}$$

In the present case, with the equilibrium concentrations determined experimentally with inductively coupled plasma optical emission spectroscopy (ICP-OES), the separation factors at pH 6.0 are: $ß_{U/La} = 121.1$ and $ß_{U/Yb} = 70.0$. The ligand **$H_2$L** therefore demonstrates promising extraction performance for the selective removal of uranyl salts from aqueous rare-earth containing solutions. As the separation factor $ß_{U/Ln}$ is ~100 in a weakly acidic pH range, a complete separation of uranyl from aqueous trivalent lanthanide solutions is expected to be achieved with few separation steps. The optimal ratio of ligand to metal in the extraction process for removing uranyl for rare-earth containing aqueous solutions was found to be 100:1 and the concentration of metal as the nitrate $\geq 10^{-4}$ mol/L. It was also found that a minimum extraction time of 10 min was required.

The extraction of lanthanides begins at pH > 5 and reaches a maximum of ca. 75% extraction at pH 7.7 (organic phase: $10^{-4}$ mol/L **$H_2$L** in $CHCl_3$; aqueous phase: $[Eu^{3+}] = 10^{-6}$ mol/L in $H_3BO_3/Na_2B_4O_7$ buffer ($10^{-2}$ mol/L in $H_2O$)). This is due to the incomplete deprotonation of the phenolic hydroxy groups at low pH values, caused by the significantly low acidity of the salicylic fragments ($pK_a \approx 8$).[38] Extractions of trivalent lanthanides cannot be realized at high pH. This is due to the formation of highly insoluble hydroxides. The solubility product of $Eu(OH)_3$ at 25 °C is $7 \cdot 10^{-27}$ (mol/L).[4] This implies that a precipitation of $Eu(OH)_3$ is already expected for concentrations of $10^{-6}$ mol/L at pH > 7.3.[41] Precipitation, however, was not observed in our buffered solution system. Up to a pH of 8.5 the lanthanide concentration of the solution was as expected. Extractions of lanthanides on a technical scale is nevertheless not recommended in the alkaline region.

The structural analysis of **$H_2$L** shows that cationic complexes are formed with trivalent lanthanides. From the interactions observed for this ligand in solution, it is expected that such species should also form during extraction processes. A phase transfer into the organic phase is therefore only possible if the counter anion is simultaneously co-extracted. The extraction in comparison to neutral complexes is therefore complicated. This is in agreement with the considerably stronger extraction of the less positively charged uranyl cation compared to the trivalent lanthanide cations. It is assumed that a neutral uranyl complex is formed during extraction. The polar binding sites around the metal cation centres are not completely screened by the hydrophobic regions of the ligand, thereby enabling additional hydrophilic interactions (Figure 8). The ligand is therefore protonated and forms 2:2 complexes. The metal centre is arranged such that the coordination of the nitrate ion functions as a co-ligand, so that a neutral complex is formed. The Van der Waals representation of the complex illustrates that the coordination environment of the cation is largely screened by the non-polar domains of the ligand system. This enables numerous hydrophobic interactions with the organic phase.

## Conclusion

The synthesis of a new tetra-substituted p-*tert*-butylcalix[4]arene ligand bearing dangling phosphoryl and salicylamide units in 1,3 and 2,4 positions as an extracting agent for *f*-element cations has been achieved. The synthesis involved a two step procedure that appends the phosphoryl- and salicylamide units in sequential steps, a route which may well be generalised to synthesize other mixed-arm extraction agents based on calix[4]arene scaffolds. The ability of **$H_2$L** to act as an efficient chelating agent for $Ln^{3+}$ cations $Ln^{3+} = La^{3+}$ (**1**), $Pr^{3+}$ (**2**), $Eu^{3+}$ (**3**), $Gd^{3+}$ (**4**), and $Yb^{3+}$ (**5**) has been demonstrated. The interaction of **$H_2$L** with $UO_2^{2+}$ has also been highlighted. X-ray crystallographic analysis of single-crystals of **1**, **3**, **4** and **6** show that the $Ln^{3+}$ cations are invariably coordinated in a tetrapodal fashion by phosphoryl O, amide O, and salicylamide O atoms from $\mathbf{L}^{2-}$. The coordination demands of the $Ln^{3+}$ ions are not fully saturated by $\mathbf{L}^{2-}$ and so the complex monomers dimerize via bridging salicylamide units and one exogenous $H_2O$ forming rod-like complexes of the type $[Ln_2\mathbf{L}_2(H_2O)]^{2+}$ with a hydrophilic seam and two hydrophobic end groups. In striking contrast, the $UO_2^{2+}$ cation is not accommodated in the binding pocket of the tetrapodal calix[4]arene ligand, but is attached to the ligand arms in an outside fashion to give a polymeric $[UO_2(\mathbf{L})(MeOH)]$

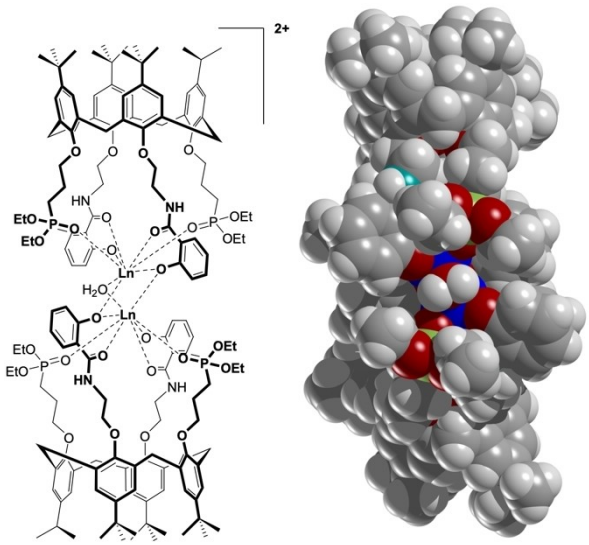


**Figure 8.** Van der Waals representation of the cationic $[Ln_2\mathbf{L}_2(\mu\text{-}H_2O)]^{2+}$ complexes.


© 2021 The Authors. Chemistry - A European Journal published by Wiley-VCH GmbH

neutral complex. **$H_2$L** was found to be an effective extracting agent for $UO_2^{2+}$ cations. The separation factors at pH 6.0 are: $ß_{U/La} = 121.1$ and $ß_{U/Yb} = 70.0$. When applied in the pH range of 4.0–5.0 only $UO_2^{2+}$ is extracted. These observations may be further exploited for the development of efficient and selective extraction agents for radioactive f-element cations.

## Experimental Section

**General procedure for the synthesis of ligands**: Unless otherwise noted, all reactions were carried out in a fumehood under ordinary atmospheric conditions. Reagent grade solvents were used without any further purification. The ligand precursor, *p-tert*-butylcalix[4]arene, was produced according to Gutsche and Iqbal.[42] Synthesis of proligand **1′** is modified slightly from Jurečka et al.[14a] and is described with additional analytical data in Supporting Information. Product purity was routinely examined by determining melting points (mp) (IA9100, Electrothermal) using open glass capillaries (100 mm × 2 mm). Elemental composition of all products were established using a VARIO EL Elemental Analyzer (Elementar Analysensysteme GmbH). All synthesised ligands assumed the *cone* formation. ATR infrared spectra were recorded on a Bruker VECTOR 22 FTIR spectrophotometer on a ZnSe crystal plate. NMR spectra were recorded on a BRUKER AVANCE DRX 400 spectrometer at 295 K ($^1$H: 400.21 MHz; $^{13}$C{$^1$H}: 100.63 MHz; $^{31}$P: 162.00 MHz). Chemical shifts refer to solvent signals for $^1$H and $^{13}$C{$^1$H} NMR spectra and to $H_3PO_4$ as an external standard for $^{31}$P NMR spectra. ESI mass spectra were recorded on a BRUKER APEX II FT-ICR spectrometer. Electronic absorption spectra were recorded on a JASCO V-570 UV/Vis/NIR spectrophotometer. The spectrophotometric data were analyzed by using the program suite HYPERQUAD2008 v1.1.33 (PROTONIC SOFTWARE).[43,44]

**5,11,17,23-Tetra-*tert*-butyl-25,27-bis[(diethoxyphosphoryl)-propoxy]-26,28-bis{2-[((2-hydroxyphenyl)carboxy)amino]ethoxy}-calix[4]arene ($H_2$L)**: Salicylic acid pentafluorophenyl ester (192 mg, 0.63 mmol, 2.3 equiv) was added to compound **1′** (300 mg, 0.27 mmol) in chloroform (25 mL) and stirred for 16 h at 45 °C. The reaction mixture was subsequently washed with 5% sodium carbonate solution (2 × 20 mL) and 1 N HCl (20 mL) and then dried over anhydrous sodium sulfate. The solvent was removed under vacuum. The residue was purified in a chromatographic column (silica gel, dichloromethane/methanol 40:1, v/v). A colourless solid was obtained, which was recrystallized from *n*-hexane, filtered, and dried to constant weight at 60 °C (204 mg colourless solid, 56% yield). Mp: 219–220 °C. Elem. anal: C 67.19, H 7.94, N 2.06 calcd [%] in $C_{76}H_{104}N_2O_{14}P_2 \cdot 1.5H_2O$, C 67.28, H 6.64, N 1.73 found [%]. ESI-MS(+) ($CH_2Cl_2$/MeOH): $m/z = 1353.7$ $[H_2L + Na^+]^+$. $^1$H NMR (400 MHz, $CD_2Cl_2$): δ [ppm] = 1.04 (s, 18H, –C(*CH*$_3$)$_3$ phosphonate-subst.), 1.14 (s, 18H, –C(*CH*$_3$)$_3$ amide-subst.), 1.27 (t, $^3J_{HH} = 7.1$ Hz, 12H, -P-(OCH$_2$*CH*$_3$)$_2$), 1.86–2.04 (m, 4H, –CH$_2$*CH*$_2$P), 2.20–2.36 (m, 4H, –*CH*$_2$CH$_2$P), 3.20 (d, $^2J_{HH} = 12.6$ Hz, 4H, ArC*H*$_{eq}$HAr), 3.93 (t, $^3J_{HH} = 7.0$ Hz, 4H, ArOC*H*$_2$CH$_2$CH$_2$P), 3.97–4.11 (m, 12H, ArOCH$_2$*CH*$_2$NH und -P(OC*H*$_2$CH$_3$)$_2$), 4.19 (t, $^3J_{HH} = 6.8$ Hz, 4H, ArOC*H*$_2$CH$_2$NH), 4.38 (d, $^2J_{HH} = 12.6$ Hz, 4H, ArCH*H*$_{ax}$Ar), 6.76 (s, 4H, calix-Ar*H* phosphonate-subst.), 6.80 (t, $^3J_{HH} = 7.6$ Hz, 2H, salicyl-4-Ar*H*), 6.89 (s, 4H, calix-Ar*H* amide-subst.); 6,90 (d, 3JHH = 10,7 Hz, 2H, salicyl-6-Ar*H*), 7.30–7.40 (m, 2H, Salicyl-5-Ar*H*), 7.87 (dd, $^3J_{HH} = 7.6$ Hz, $^4J_{HH} = 1.6$ Hz, 2H, salicyl-3-Ar*H*), 8.58 (br, 2H, N*H*), 12.61 (br, 2H, –O*H*). $^{13}$C{$^1$H} NMR (101 MHz, $CD_2Cl_2$): δ [ppm] = 16.8 (d, $^3J_{CP} = 5.8$ Hz, -POCH$_2$*CH*$_3$), 22.7 (d, $^1J_{CP} = 142$ Hz, –CH$_2$*CH*$_2$P), 23.9 (d, $^2J_{CP} = 4.6$ Hz, –CH$_2$CH$_2$P), 31.6 (ArCH$_2$Ar), 31.7 (–C(*CH*$_3$)$_3$ phosphonate-subst.), 31.8 (–C(*CH*$_3$)$_3$ amid-subst.), 34.3 (–*C*(CH$_3$)$_3$ phosphonate-subst.), 34.4 (–*C*(CH$_3$)$_3$ amide-subst.), 40.9 (ArOCH$_2$*CH*$_2$N), 62.6 (d, $^2J_{CP} = 6.7$ Hz, –POCH$_2$CH$_3$), 72.9 (ArO*CH*$_2$CH$_2$N), 75.7 (d, $^3J_{CP} = 20.4$ Hz, ArOCH$_2$CH$_2$*CH*$_2$P), 115.8 (salicyl-2-$C_{Ar}$), 118,4 (salicyl-6-*C*Ar), 118.9 (salicyl-4-$C_{Ar}$); 125,7 (calix-$C_{Ar}$–H phosphonate-subst.); 126,0 (calix-$C_{Ar}$–H amide-subst.), 127.8 (salicyl-3-$C_{Ar}$), 133.8 (calix-$C_{Ar}$–$CH_2$ phosphonate-subst.), 134,1 (salicyl-5-$C_{Ar}$), 134.5 (calix-$C_{Ar}$–$CH_2$ amide-subst.), 145.4 (calix-$C_{Ar}$–$^t$Bu phosphonate-subst.), 145.8 (calix-$C_{Ar}$–$^t$Bu amide-subst.), 153.7 ($C_{Ar}$–OCH$_2$CH$_2$CH$_2$P), 153.9 ($C_{Ar}$–OCH$_2$CH$_2$N), 161.8 (salicyl-1- $C_{Ar}$), 171.2 (*C*=O). $^{31}$P NMR (162 MHz, $CD_2Cl_2$): δ [ppm] = 32.4. ATR-IR (ZnSe): $\tilde{\nu}$ [cm$^{-1}$] = 3296 br (ν N–H, ν O–H), 2960 s, 2906 m, 1642 m (ν C=O), 1593 m, 1550 m (δ C–N–H), 1517 w, 1481 s, 1391 w, 1361 m, 1304 w, 1233 s (ν P=O), 1198 s, 1148 m, 1124 m, 1098 w, 1024 s, 963 s, 870 w, 826 m, 786 w, 755 m, 697 w, 664 w. UV-vis (MeCN): $\lambda_{max}$ [nm] (ε [M$^{-1}\cdot$cm$^{-1}$]) = 203 (141600), 287 (sh), 303 (9890).

**General procedure for the synthesis of lanthanide (III) complexes with $H_2$L**: The complexing ligand, **$H_2$L** (60.0 mg, 45.1 μmol) is dissolved in methanol (2 mL), to which sodium methanolate (7.3 mg, 135 μmol) is added. Trivalent lanthanide nitrate salt (47.3 μmol, 1.05 equiv) in methanol (1 mL) is added to this reaction mixture and stirred at room temperature for 16 h. Subsequently, sodium tetraphenyl borate (154 mg, 451 μmol, 10 equiv) dissolved in methanol (1 mL) is added and the reaction mixture stirred for another 16 h at room temperature. The solid material that formed was removed from solution by filtration and dried to constant weight at 60 °C. The CHN analytical data of the initially isolated complexes were modelled assuming the presence of various amounts of co-crystallized $H_2O$ molecules (9 for **1**, 2 for **2**, 5.5 for **3**, 5 for **4**, 3 for **5**). The presence of co-crystallized $H_2O$ is reasonable, given that large voids are present in the crystal structures (see below). When recrystallized from MeOH/$CH_2Cl_2$, the $H_2O$ molecules are replaced by MeOH molecules.

**[La$_2$L$_2$(μ-H$_2$O)](BPh$_4$)$_2$ – (1)**: The complex is synthesised according to the general procedure using $La(NO_3)_3 \cdot 6H_2O$ (20.5 mg). A colourless solid was obtained (39.7 mg, 49% yield). Mp: 220 °C (decomp). Elem. anal: C 63.96, H 7.07, N 1.49 calcd [%] in $C_{200}H_{246}B_2La_2N_4O_{29}P_4 \cdot 9H_2O$, C 63.88, H 6.73, N 1.20 found [%]. ESI-MS(+) ($CH_2Cl_2$/MeCN): $m/z = 1468.1$ $[La_2L_2]^{2+}$. ATR-IR (ZnSe): $\tilde{\nu}$ [cm$^{-1}$] = 3427 m (ν N–H), 3381 m (ν N–H), 3056 m, 3038 w, 2961 s, 2905 m, 2866 m, 1607 s (ν C=O), 1581 m, 1532 m (δ C–N–H), 1480 s, 1441 m, 1427 w, 1393 w, 1361 m, 1309 w, 1266 m, 1241 m, 1194 s, 1123 m, 1053 s, 1029 s, 976 m, 870 w, 835 m, 762 w, 745 w, 733 m, 703 s. UV-vis (MeCN): $\lambda_{max}$ [nm] (ε [M$^{-1}\cdot$cm$^{-1}$]) = 197 (443186), 323 (21866).

**[Pr$_2$L$_2$(μ-H$_2$O)](BPh$_4$)$_2$ – (2)**: The complex is synthesised according to the general procedure using $Pr(NO_3)_3 \cdot 6H_2O$ (20.7 mg). A colourless solid was obtained (53.6 mg, 66% yield). Mp: 218 °C (decomp). Elem. anal: C 66.11, H 6.94, N 1.54 calcd [%] in $C_{200}H_{246}B_2N_4O_{29}P_4Pr_2 \cdot 2H_2O$, C 66.02, H 6.74, N 1.25 found [%]. ESI-MS(+) ($CH_2Cl_2$/MeCN): $m/z = 1470.1$ $[Pr_2L_2]^{2+}$. ATR-IR (ZnSe): $\tilde{\nu}$ [cm$^{-1}$] = 3373 m (ν N–H), 3055 m, 3040 w, 2962 s, 2905 m, 2867 m, 1608 s (ν C=O), 1582 m, 1534 m (δ C–N–H), 1479 s, 1441 m, 1393 w, 1361 w, 1308 m, 1266 w, 1241 m, 1226 m, 1194 s, 1123 m, 1053 s, 1029 s, 976 m, 870 w, 836 m, 763 w, 745 w, 732 m, 703 s. UV-vis (MeCN): $\lambda_{max}$ [nm] (ε [M$^{-1}\cdot$cm$^{-1}$]) = 196 (597454), 324 (22738).

**[Eu$_2$L$_2$(μ-H$_2$O)](BPh$_4$)$_2$ – (3)**: The complex is synthesised according to the general procedure using $Eu(NO_3)_3 \cdot 6H_2O$ (21.1 mg). A pale yellow solid was obtained (64.0 mg, 78% yield). Mp: 223 °C (decomp). Elem. anal: C 64.60, H 6.97, N 1.51 calcd [%] in $C_{200}H_{246}B_2Eu_2N_4O_{29}P_4 \cdot 5.5H_2O$, C64.62, H 6.78, N 1.21 found [%]. ESI-MS(+) ($CH_2Cl_2$/MeCN): $m/z = 1481.6$ $[Eu_2L_2]$. ATR-IR (ZnSe): $\tilde{\nu}$ [cm$^{-1}$] = 3445 m (ν N–H), 3053 m, 3039 w, 2960 s, 2905 m, 2865 m, 1608 s (ν C=O), 1581 m, 1536 m (δ C–N–H), 1479 s, 1441 m, 1392 w, 1362 w, 1308 m, 1265 w, 1239 m, 1226 m, 1194 s, 1123 m, 1051 s, 1023 s, 974 m, 870 w, 835 m, 801 w, 760 w, 732 m, 703 s. UV-vis (MeCN): $\lambda_{max}$ [nm] (ε [M$^{-1}\cdot$cm$^{-1}$]) = 196 (360000), 324 (13726).


© 2021 The Authors. Chemistry - A European Journal published by Wiley-VCH GmbH

**$[Gd_2L_2(\mu\text{-}H_2O)](BPh_4)_2$ – (4)**: The complex is synthesised according to the general procedure using $Gd(NO_3)_3 \cdot 6H_2O$ (21.3 mg). A colourless solid was obtained (74.2 mg, 91% yield). Mp: 230 °C (decomp). Elem. anal: C 64.57, H 6.94, N 1.51 calcd [%] in $C_{200}H_{246}B_2Gd_2N_4O_{29}P_4 \cdot 5H_2O$, C 64.56, H 6.75, N 1.25 found [%]. ESI-MS(+) ($CH_2Cl_2$/MeCN): $m/z = 1486.6$ $[Gd_2L_2]$. ATR-IR (ZnSe): $\tilde{\nu}$ [$cm^{-1}$] = 3382 m ($\nu$ N–H), 3056 m, 3034 w, 2959 s, 2906 m, 2867 m, 1609 s ($\nu$ C=O), 1583 m, 1535 m ($\delta$ C–N–H), 1479 s, 1441 m, 1393 w, 1361 w, 1331 w, 1308 m, 1266 w, 1241 m, 1225 m, 1194 s, 1123 m, 1053 s, 1029 s, 976 m, 869 w, 836 m, 764 w, 745 w, 732 m, 703 s. UV-vis (MeCN): $\lambda_{max}$ [nm] ($\varepsilon$ [$M^{-1} \cdot cm^{-1}$]) = 198 (838300), 321 (33500).

**$[Yb_2L_2(\mu\text{-}H_2O)](BPh_4)_2$ – (5)**: The complex is synthesized according to the general procedure using $Yb(NO_3)_3 \cdot 5H_2O$ (21.2 mg). A colourless solid was obtained (74.2 mg, 80% yield). Mp: 219 °C (decomp). Elem. anal: C 64.65, H 6.84, N 1.51 calcd [%] in $C_{200}H_{246}B_2Yb_2N_4O_{29}P_4 \cdot 3H_2O$, C 64.73, H 6.25, N 1.25 found [%]. ESI-MS(+) ($CH_2Cl_2$/MeCN): $m/z = 1502.6$ $[Yb_2L_2]$. ATR-IR (ZnSe): $\tilde{\nu}$ [$cm^{-1}$] = 3384 m ($\nu$ N–H), 3056 m, 2963 s, 2904 m, 2868 m, 1609 s ($\nu$ C=O), 1580 m, 1540 m ($\delta$ C–N–H), 1478 s, 1442 m, 1393 w, 1362 w, 1331 w, 1266 w, 1243 m, 1187 s, 1123 m, 1026 s, 974 m, 869 w, 845 m, 7635w, 703 s. UV-vis (MeCN): $\lambda_{max}$ [nm] ($\varepsilon$ [$M^{-1} \cdot cm^{-1}$]) = 195 (605500), 324 (14250).

### Synthesis of uranyl complex with $H_2L$

**$[(UO_2)L_2(MeOH)]_n$ – (6)**: Uranyl(VI) acetate dihydrate (12.6 mg, 29.7 μmol, 1.0 equiv) was dissolved in methanol (0.5 mL) and added to a solution of **$H_2L$** (39.6 mg, 29.7 μmol) in methanol (1 mL). This intense orange coloured solution is stirred at room temperature for 16 h. The solid that formed was removed by filtration, washed with a little methanol (cold) and subsequently dried to constant weight at 60 °C (33.1 mg intense yellow crystals, 69% yield). Mp: > 250 °C (decomp). Elem. anal: C 56.68, H 6.55, N 1.72 calcd [%] in $C_{77}H_{106}N_2O_{17}P_2U$, C 56,73, H 6.41, N 1.67 found [%]. ESI-MS(+) (MeOH): $m/z = 1621.7$ $[(UO_2)L + Na^+]^+$. ATR-IR (KBr): $\tilde{\nu}$ [$cm^{-1}$] = 3429 br, 3058 w, 2962 s, 2906 m, 2868 m, 1645 m ($\nu$ C=O), 1610 m ($\nu$ C=O), 1582 m, 1541 m ($\delta$ C–N–H), 1481 s, 1469 m, 1448 m, 1392 m, 1362 m, 1312 m, 1247 s, 1200 s, 1149 w, 1100 w, 1025 s, 970 m, 904 m, 870 w, 825 w, 759 m, 700 w, 636 w, 585 w, 540 w.

**Crystallography**: X-ray diffraction data for the free ligand **$H_2L$**·3MeCN and the complexes **1**·14MeOH, **3**·12MeOH, **4**·13MeOH and **6**·5MeOH were recorded on a IPDS-2T image plate detector system equipped with a sealed X-ray tube (Mo-$K_\alpha$ radiation, $\lambda$ = 71.073 pm). The data sets were processed with the program STOE X-AREA.[45] The structures were solved by direct methods or Patterson methods and refined using SHELX 2018.[46] The non-hydrogen atoms of the framework were refined anisotropically. The coordinates of the hydrogen atoms of the framework were calculated for idealized positions. In the present structures additional MeOH solvent molecules occupy interstitial spaces that are generated by packing, and as a result are highly disordered. As this disorder was sufficiently bad to prevent modelling, the routine SQUEEZE implemented in Platon[47] was applied to remove this diffuse electron density. The total potential solvent accessible void volume per unit cell is 2010 Å$^3$ (for **1**), 1881 Å$^3$ (for **3**), 2008 Å$^3$ (for **4**), and 2758 Å$^3$ (for **6**). The total amount of diffuse electrons per unit cell amounts to 493 $e^-$ (for **1**), 428 $e^-$ (for **3**), 459 $e^-$ (for **4**), and 718 $e^-$ (for **6**). This corresponds to 14 (for **1**), 12 (for **3**), 13 (for **4**), and 5 (for **6**) methanol molecules per formula unit. The programs DIAMOND 3.2i, Ortep-III and POV-Ray v3.7 were used for drawings.[48–50]

Deposition Number(s) 2085835 (for $H_2L$), 2085836 (for **1**·14MeOH), 2085837 (for **3**·12MeOH), 2085838 (for **4**·13MeOH), 2085839 (for **6**·5MeOH) contain(s) the supplementary crystallographic data for this paper. These data are provided free of charge by the joint Cambridge Crystallographic Data Centre and Fachinformationszentrum Karlsruhe Access Structures service.

**Liquid-liquid-extraction**: Extraction experiments and competitive extraction with lanthanum (III) and ytterbium (III) nitrate were performed using chloroform as the organic phase and a 0.01 mol·$L^{-1}$ boric acid/sodium borate buffer solution as aqueous phase. The concentration of the metal salts was held constant ($1 \cdot 10^{-4}$ mol·$L^{-1}$), while the concentration of the ligand was varied ($c = 0–1 \cdot 10^{-2}$ mol·$L^{-1}$). An amount of 1 mL of each of the two phases were combined in a vial and shaken at room temperature for 15 min at 1200 rpm on a platform shaker. The pH of the aqueous solution was checked before and after the extraction. The mixtures were allowed to stand for 30 min to ensure equilibration. Aliquots of the aqueous phase were subsequently taken, diluted and acidified to pH ≈ 1.2 with $HNO_3$. The residual metal content in this aqueous phase was quantified using ICP-OES measurements using a Perkin-Elmer OPTIMA8000 or Elan 9000 ICP-OES instrument.

## Supporting Information

Contains the X-ray crystal structures of all new compounds (in cif-format), the associated characterization data, as well as spectrophotometric titrations of $H_2L$ with $Ln(NO_3)_3$.

## *Acknowledgements*

Prof. Dr. H. Krautscheid is gratefully acknowledged for providing the facilities for X-ray crystallographic measurements. The authors thank Dr. M. Börner for recording the diffuse reflectance spectra and for X-ray analysis. This work was funded within the framework of r$^4$-Innovative Technologies for Resource Efficiency, German Federal Ministry of Education and Research (Project: SEFLECX; funding code: 033R132 D). Open Access funding enabled and organized by Projekt DEAL.

## Conflict of Interest

The authors declare no conflict of interest.

## Data Availability Statement

The data that support the findings of this study are available from the corresponding author upon reasonable request.

**Keywords:** actinides · calixarene · lanthanides · solvent extraction · uranyl

[1] T. Lorenz, M. Bertau, *J. Cleaner Prod.* **2019**, *215*, 131–143.
[2] J. Gambogi, in U. S. Geological Survey, Mineral commodity summaries, **2021**, *2021*, 132–133.
[3] A. R. Chakhmouradian, F. Wall, *Elements* **2012**, *8*, 333–340.
[4] Y. Lu, W. Liao, *Hydrometallurgy* **2016**, *165*, 300–305.
[5] E. J. Werner, S. M. Biros, *Org. Chem. Front.* **2019**, *6*, 2067–2094.


© 2021 The Authors. Chemistry - A European Journal published by Wiley-VCH GmbH

[6] J. A. Mattocks, J. A. Cotruvo, *Chem. Soc. Rev.* **2020**, *49*, 8315–8334.

[7] a) J. A. Bogart, C. A. Lippincott, P. J. Carroll, E. J. Schelter, *Angew. Chem. Int. Ed.* **2015**, *54*, 8222–8225; *Angew. Chem.* **2015**, *127*, 8340–8343; b) B. E. Cole, T. Cheisson, R. F. Higgins, E. Nakamaru-Ogiso, B. C. Manor, P. J. Carroll, E. J. Schelter, *Inorg. Chem.* **2020**, *59*, 172–178; c) J. J. M. Nelson, T. Cheisson, H. J. Rugh, M. R. Gau, P. J. Carroll, E. J. Schelter, *Commun. Chem.* **2020**, *3*, 7.

[8] J.-P. A. Renier, M. L. Grossbeck, in Development of Improved Burnable Poisons for commercial nuclear power reactors, Oak Ridge National Laboratory, Oak Ridge, Tennessee, **2001**.

[9] B. Mokhtari, K. Pourabdollah, N. Dallali, *J. Radioanal. Nucl. Chem.* **2011**, *287*, 921–934.

[10] M. J. Hudson, L. M. Harwood, D. M. Laventine, F. W. Lewis, *Inorg. Chem.* **2013**, *52*, 3414–3428.

[11] H. H. Dam, D. N. Reinhoudt, W. Verboom, *Chem. Soc. Rev.* **2007**, *36*, 367–377.

[12] a) B. M. Furphy, J. M. Harrowfield, D. L. Kepert, B. W. Skelton, A. H. White, F. R. Wilner, *Inorg. Chem.* **1987**, *26*, 4231–4236; b) B. S. Creaven, D. F. Donlon, J. McGinley, *Coord. Chem. Rev.* **2009**, *253*, 893–962; c) D. T. Schühle, J. A. Peters, J. Schatz, *Coord. Chem. Rev.* **2011**, *255*, 2727–2745; d) R. Joseph, C. P. Rao, *Chem. Rev.* **2011**, *111*, 4658–4702; e) R. Gramage-Doria, D. Armspach, D. Matt, *Coord. Chem. Rev.* **2013**, *257*, 776–816; f) M. A. McKervey, F. Arnaud-Neu, M.-J. Schwing-Weill, in: *Comprehensive Supramolecular Chemistry* (Ed.: G. W. Gokel), Pergamon, Oxford, **1996**; g) W. Sliwa, T. Girek, *J. Inclusion Phenom. Macrocyclic Chem.* **2010**, *66*, 15–41.

[13] a) M. R. Yaftian, M. Burgard, D. Matt, C. B. Dieleman, F. Rastegar, *Solvent Extr. Ion Exch.* **1997**, *15*, 975–989; b) P. D. Beer, M. G. B. Drew, M. Kan, P. B. Leeson, M. I. Ogden, G. Williams, *Inorg. Chem.* **1996**, *35*, 2202–2211; c) F. Arnaud-Neu, V. Böhmer, J.-F. Dozol, C. Grüttner, R. A. Jakobi, D. Kraft, O. Mauprivez, H. Rouquette, M.-J. Schwing-Weill, N. Simon, W. Vogt, *J. Chem. Soc. Perkin Trans. 2* **1996**, 1175–1182; d) S. Barboso, A. G. Carrera, S. E. Matthews, F. Arnaud-Neu, V. Böhmer, J.-F. Dozol, H. Rouquette, M.-J. Schwing-Weill, *J. Chem. Soc. Perkin Trans. 2* **1999**, 719–724; e) V. R. Sastri, J. R. Perumareddi, V. R. Rao, G. V. S. Rayudu, J.-C. G. Bünzli, in *Modern Aspects of Rare Earths and Their Complexes;* Elsevier, Amsterdam, **2003**; f) M. Wehbie, G. Arrachart, L. Ghannam, I. Karamé, S. Pellet-Rostaing, *Dalton Trans.* **2017**, *46*, 16505–16515.

[14] a) P. Jurečka, P. Vojtíšek, K. Novotný, J. Rohovec, I. Lukeš, *J. Chem. Soc.-Perkin Trans.* **2002**, *2*, 1370–1377; b) S. R. Menon, J. A. R. Schmidt, *Tetrahedron* **2016**, *72*, 767–774; c) I. Vatsouro, A. Serebryannikova, L. Wang, V. Hubscher-Bruder, E. Shokova, M. Bolte, F. Arnaud-Neu, V. Böhmer, V. Kovalev, *Tetrahedron* **2011**, *67*, 8092–8101; d) A. B. Chetry, T. Matsufuji, B. B. Adhikari, S. Morisada, H. Kawakita, K. Ohto, T. Oshima & Jumina, *J. Inclusion Phenom. Macrocyclic Chem.* **2015**, *81*, 301–310.

[15] K. Ohto, M. Yano, K. Inoue, T. Yamamoto, M. Goto, F. Nakashio, S. Shinkai, T. Nagasaki, *Anal. Sci.* **1995**, *11*, 893–902.

[16] a) A. Casnati, N. Della Ca', M. Fontanella, F. Sansone, F. Ugozzoli, R. Ungaro, K. Liger, J.-F. Dozol, *Eur. J. Org. Chem.* **2005**, *2005*, 2338–2348; b) A. Casnati, L. Baldini, F. Sansone, R. Ungaro, N. Armaroli, D. Pompei, F. Barigelletti, *Supramol. Chem.* **2002**, *14*, 281–289.

[17] a) M. Karavan, F. Arnaud-Neu, V. Hubscher-Bruder, I. Smirnov, V. Kalchenko, *J. Inclusion Phenom. Macrocyclic Chem.* **2010**, *66*, 113–123; b) M. Tanaka, S. Morisada, H. Kawakita, K. Inoue, K. Ohto, *J. Inclusion Phenom. Macrocyclic Chem.* **2015**, *82*, 33–41; c) S. A. Ansari, P. K. Mohapatra, A. Sengupta, N. I. Nikishkin, J. Huskens, W. Verboom, *Eur. J. Inorg. Chem.* **2014**, *2014*, 5689–5697; d) S. A. Ansari, P. K. Mohapatra, W. Verboom, Z. Zhang, P. D. Dau, J. K. GibAnsarison, L. Rao, *Dalton Trans.* **2015**, *44*, 6416–6422; e) P. K. Mohapatra, A. Sengupta, M. Iqbal, J. Huskens, W. Verboom, *Inorg. Chem.* **2013**, *52*, 2533–2541; f) N. E. Borisova, A. A. Kostin, E. A. Eroshkina, M. D. Reshetova, K. A. Lyssenko, E. N. Spodine, L. N. Puntus, *Eur. J. Inorg. Chem.* **2014**, *2014*, 2219–2229; g) M. Regueiro-Figueroa, J. L. Barriada, A. Pallier, D. Esteban-Gómez, A. d Blas, T. Rodríguez-Blas, É. Tóth, C. Platas-Iglesias, *Inorg. Chem.* **2015**, *54*, 4940–4952.

[18] H. Huang, S. Ding, N. Liu, Y. Wu, D. Su, S. Huang, *Sep. Purif. Technol.* **2014**, *123*, 235–240.

[19] A. Jäschke, M. Kischel, A. Mansel, B. Kersting, *Eur. J. Inorg. Chem.* **2017**, *2017*, 894–901.

[20] N. Schreiter, P. Fröhlich, M. Bertau, Presentation at annual meeting of ProcessNet, Extraction and Processing, Frankfurt, Germany, 12.03.2018.

[21] Q. I. Roode-Gutzmer, L. N. Holderied, F. Glasneck, B. Kersting, P. Fröhlich, M. Bertau, *Org. Process Res. Dev.* **2019**, *23*, 2425–2438.

[22] A. Bauer, A. Jäschke, S. Schöne, R. Barthen, J. März, K. Schmeide, M. Patzschke, B. Kersting, K. Fahmy, J. Oertel, V. Brendler, T. Stumpf, *ChemistryOpen* **2018**, *7*, 467–474.

[23] F. Glasneck, K. Kobalz, B. Kersting, *Eur. J. Inorg. Chem.* **2016**, *2016*, 3111–3122.

[24] a) S. Ullmann, P. Hahn, P. Mini, K. L. Tuck, A. Kahnt, B. Abel, M. E. Gutierrez Suburu, C. A. Strassert, B. Kersting, *Dalton Trans.* **2020**, *49*, 11179–11191; b) P. Hahn, S. Ullmann, A. Kahnt, B. Abel, B. Kersting, *Inorg. Chim. Acta* **2020**, *514*, 119983.

[25] A. Filarowski, *J. Phys. Org. Chem.* **2005**, *18*, 686–698.

[26] G. E. Dunn, F. Kung, *Can. J. Chem.* **1966**, *44*, 1261–1269.

[27] G. A. Jeffrey, W. Saenger, *Hydrogen bonding in Biological Structures*, Springer-Verlag, Berlin Heidelberg, **1994**.

[28] A. Pedretti, L. Villa, G. Vistoli, VEGA: A versatile program to convert, handle and visualize molecular structure on Windows-based PCs. *J. Mol. Graph. Model.* **2002**, *21*, 47–49.

[29] S. Mecozzi, J. Rebek Jr., *Chem. Eur. J.* **1998**, *4*, 1016–1022.

[30] M. Llunell, D. Casanova, J. Cirera, P. Alemany, S. Alvarez, *SHAPE*, University of Barcelona, **2013**.

[31] F. Habib, G. Brunet, V. Vieru, I. Korobkov, L. F. Chibotaru, M. Murugesu, M. J. Am, *Chem. Soc. Rev.* **2013**, *135*, 13242–13245.

[32] Y. Jiang, R. J. Holmberg, F. Habib, L. Ungur, I. Korobkov, L. F. Chibotaru, M. Murugesu, *RSC Adv.* **2016**, *6*, 56668–56673.

[33] M. Seitz, A. G. Oliver, K. N. Raymond, *J. Am. Chem. Soc.* **2007**, *129*, 11153–11160.

[34] F. Berny, N. Muzet, L. Troxler, A. Dedieu, G. Wipff, *Inorg. Chem.* **1999**, *38*, 1244–1252.

[35] S. V. Krivovichev, P. C. Burns, I. G. Tananaev, in *Structural chemistry of inorganic actinide compounds*, 1st ed, Elsevier, Netherlands, **2007**.

[36] A. G. Orpen, L. Brammer, F. H. Allen, O. Kennard, D. G. Watson, R. Taylor, *J. Chem. Soc. Dalton Trans.* **1989**, S1–S83.

[37] N. G. Tsierkezos, A. I. Phillippopoulous, *Fluid Phase Equilib.* **2009**, *277*, 20–28.

[38] Z. Rappoport, in *CRC Handbook of Tables for Organic Compounds Identification*, CRC Press, Boca Raton, USA, **1995**.

[39] L. J. Charbonnière, C. Balsiger, K. J. Schenk, J.-C. G. Bünzli, *J. Chem. Soc. Dalton Trans.* **1998**, 505–510.

[40] J. H. Yoe, A. E. Harvey, *J. Am. Chem. Soc.* **1948**, *70*, 648–654.

[41] D. E. Chirkst, O. L. Lobacheva, I. V. Berlinskii, *Russ. J. Phys. Chem. A* **2010**, *84*, 2047–2050.

[42] C. D. Gutsche, M. Iqbal, *Org. Synth.* **1990**, *68*, 234.

[43] P. Gans, A. Sabatini, A. Vacca, *Hyperquad2008*, Protonic Software, Leeds, West Yorkshire, UK, **2008**.

[44] P. Gans, A. Sabatini, A. Vacca, *Talanta* **1996**, *43*, 1739–1753.

[45] X-AREA, *X-AREA*, Stoe & Cie GmbH, Darmstadt, Germany, **2006**.

[46] G. M. Sheldrick, *Acta Crystallogr. Sect. C* **2015**, *71*, 3–8.

[47] A. L. Spek, *PLATON – A Multipurpose Crystallographic Tool*, Utrecht University, Utrecht, The Netherlands, **2000**.

[48] K. Brandenburg, *DIAMOND 3.2*, Crystal Impact GbR, Bonn, Germany, **2010**.

[49] M. N. Burnett, C. K. Johnson, ORTEP-III: Oak Ridge Thermal Ellipsoid Plot Program for crystal structure illustrations. ORNL-6895, 369685, **1996**.

[50] *Persistence of Vision Pty. Ltd.*, Persistence of Vision Pty. Ltd., Williams-town, Australia.


Manuscript received: December 2, 2021
Accepted manuscript online: December 26, 2021
Version of record online: January 27, 2022



© 2021 The Authors. Chemistry - A European Journal published by Wiley-VCH GmbH